ACS OMEGA

http://pubs.acs.org/journal/acsodf

Article

Synthesis and Characterization of Co−ZnO and Evaluation of Its Photocatalytic Activity for Photodegradation of Methyl Orange

Muhammad Adeel, Muhammad Saeed,* Iltaf Khan, Majid Muneer, and Nadia Akram

Cite This: *ACS Omega* 2021, 6, 1426−1435

Read Online

ACCESS | Metrics & More | Article Recommendations

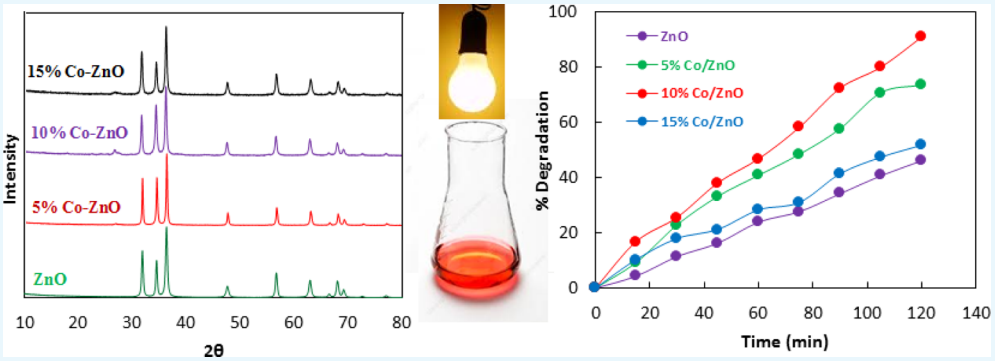

ABSTRACT: Photocatalysis is one of the techniques used for the eradication of organic pollutants from wastewater. In this study, Co−ZnO was tested as a photocatalyst for the degradation of methyl orange under irradiation of visible light. Co−ZnO loaded with 5%, 10%, and 15% Co was prepared by the precipitation method. The advanced techniques including X-ray diffraction, X-ray photoelectron spectroscopy, diffuse reflectance UV−visible spectroscopy, photoelectrochemical measurements, temperature-programmed desorption, photoluminescence, and fluorescence spectroscopy related to $OH^{\bullet}$ measurements were used for characterization of prepared Co−ZnO. Experiments showed that 10% Co−ZnO was a highly efficient catalyst for the photodegradation of methyl orange as compared to ZnO. The enhanced photocatalytic activity of Co−ZnO is attributed to the implantation of Co which inhibits the electron−hole recombination. A 100 mg/L solution of methyl orange dye was completely degraded within 130 min. The reaction kinetics has been described in terms of the Eley−Rideal mechanism.

1. INTRODUCTION

Synthetic dyes, which are used in huge amounts in the textile industry, are chemically and physically stable compounds which are harmful to the environment. Due to stability and solubility in water, synthetic dyes pile up in industrial effluents and wastewater.[1−3] Several conventional methods including biological treatment, anaerobic, aerobic, electrochemical, oxidation, reduction, flotation, flocculation, precipitation, adsorption, and so forth have been used for the treatment of wastewater; however, these methods cannot completely degrade the organic pollutants.[4−9] Therefore, photodegradation of organic pollutants with semiconductor metal oxides is a promising protocol for water purification because it has shown considerable performance for degradation of a wide range of toxic and nondegradable organic pollutants in wastewater without involving complex technologies.[10] Photocatalytic degradation under irradiation of visible light is a suitable option for the eradication of recalcitrant pollutants from water. ZnO is environmentally friendly and abundant-in-nature semiconductors with n-type conductivity and a wide band gap of 3.3 eV. These characteristics make ZnO a promising material for a number of applications, that is, gas sensors, antibacterial coatings, electrical devices, optical coatings, solar cells, and photocatalysts.[11] Due to good quantum efficiency, wide band gap, and nontoxic nature, ZnO has been extensively used in the photocatalytic degradation of organic pollutants. When ZnO is irradiated, a pair of positive holes and electrons is generated in the valence band and conduction band. The secondary reactions of the positive hole and electron generate OH radicals. The OH radical which is an influential oxidizer reacts with organic pollutants and degrades it.[12] However, the wider band gap, 3.3 eV, ZnO cannot be used as a photocatalyst under visible irradiation.[13,14] An efficient photocatalyst should absorb not only ultraviolet radiation but visible radiation as well because the solar radiation is composed of 45% visible

Received: October 19, 2020
Accepted: December 29, 2020
Published: January 5, 2021

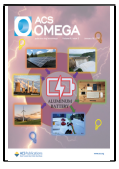

radiation and less than 10% ultraviolet radiation in addition to other types of radiations.[15] The efficiency of ZnO to absorb the visible radiation can be enhanced by narrowing the band gap or dividing it into many subgaps. The implantation of transition metal ions in the structure of ZnO is one of the techniques used for narrowing the band gap.[16,17] The implanting metals normally occupy the positions located between the VB and CB of ZnO. The photogenerated carriers are trapped at these localized positions, and the recombination rate is decreased which ultimately enhances the photocatalytic activity of ZnO.[18] Many researchers have evaluated the photocatalytic efficiency of metal-doped ZnO nanoparticles. Shkir et al. have investigated the photocatalytic efficiency of Tb−ZnO and Sr−ZnO.[19,20] Chandekar and co-workers have developed La−ZnO as an active photocatalyst by the flash combustion route.[21] Similarly, other researchers have implanted other metals such as La, Mn, Bi, Fe, and Cu on ZnO for the improvement in photocatalytic efficiency of ZnO.[22−26] Herein, we report the visible-light-driven photodegradation of methyl orange in the presence of a Co−ZnO photocatalyst. Although many researchers have prepared Co−ZnO, however, the photodegradation of methyl orange in the presence of the Co−ZnO catalyst has not been investigated extensively. The implantation of Co ions in ZnO is expected to alter the light absorption behavior and create defects in ZnO. The creation of defects will increase the visible light harvesting ability of ZnO by narrowing the band gap.

2. EXPERIMENTAL SECTION

2.1. Synthesis of ZnO. A solution of oxalic acid dihydrate, $(COOH)_2{\cdot}2H_2O$, was prepared by dissolving 3.78 g of oxalic acid dehydrate, $(COOH)_2{\cdot}2H_2O$, in 50 mL of deionized water. Another solution was prepared by dissolving 3.38 g of zinc acetate dihydrate, $Zn(CH_3COO)_2{\cdot}2H_2O$, in 50 mL of deionized water. Both solutions were mixed and stirred at 60 °C for 5 h. The precipitated zinc oxalate was filtered, washed, and dried at 100 °C for 12 h. Finally, the dried zinc oxalate was calcined at 450 °C to get zinc oxide, ZnO.

2.2. Synthesis of Co−ZnO. The chemical precipitation method was used for the synthesis of cobalt-doped zinc oxide, Co−ZnO. For this purpose, a solution was prepared by dissolving 4.38 g of zinc acetate dehydrate, $Zn(CH_3COO)_2{\cdot}2H_2O$, in 50 mL of deionized water. Similarly, another solution of cobalt nitrate hexahydrate, $Co(NO_3)_2{\cdot}6H_2O$, was prepared by adding 0.33 g of $Co(NO_3)_2{\cdot}6H_2O$ in 30 mL of deionized water. Then, both solutions were mixed and 2 M NaOH was added drop-wise to the mixture. After stirring for 2 h, the resultant precipitate was filtered, washed, and dried at 100 °C for 12 h. Finally, the obtained solid was calcined at 450 °C to get 5% Co−ZnO. The same procedure was used for the preparation of 10% Co−ZnO and 15% Co−ZnO using 0.66 and 0.99 g of $Co(NO_3)_2{\cdot}6H_2O$ as a source of Co, respectively.

2.3. Characterization. X-ray diffraction (XRD), X-ray photoelectron spectroscopy (XPS), diffuse reflectance UV−visible (DR-UV−vis) spectroscopy, photoelectrochemical (PEC) measurements, temperature programmed desorption (TPD), photoluminescence (PL) and fluorescence spectroscopy related to $OH^{\bullet}$ measurements were used for characterization of the prepared material. A Bruker D8 (Germany), Kratos Axis Ultra DLD apparatus, Shimadzu model UV-2550 spectrometer, AutoChem TP 5080 chemisorption analyzer, and PerkinElmer LS55 spectrofluorometer were used for XRD analyses, XPS analyses, DR-UV−vis analyses, TPD analyses, and fluorescence spectroscopy related to $OH^{\bullet}$ measurements, respectively.

2.4. Photocatalytic Experiment. The photocatalytic activities of as-prepared ZnO and Co−ZnO samples were tested by photodegradation of methyl orange. Typically, photodegradation of methyl orange was performed by stirring a reaction mixture composed of 0.05 g of catalyst per 50 mL of dye solution under irradiation of visible light. Before irradiation, the reaction mixture was equilibrated by stirring in dark for 30 min. Then, the mixture was magnetically stirred under irradiation of visible light. The extent of photodegradation was measured with a UV−vis spectrophotometer.

3. RESULTS AND DISCUSSION

3.1. X-ray Diffraction. XRD patterns of ZnO and Co−ZnO samples are given in Figure 1. All the diffraction peaks

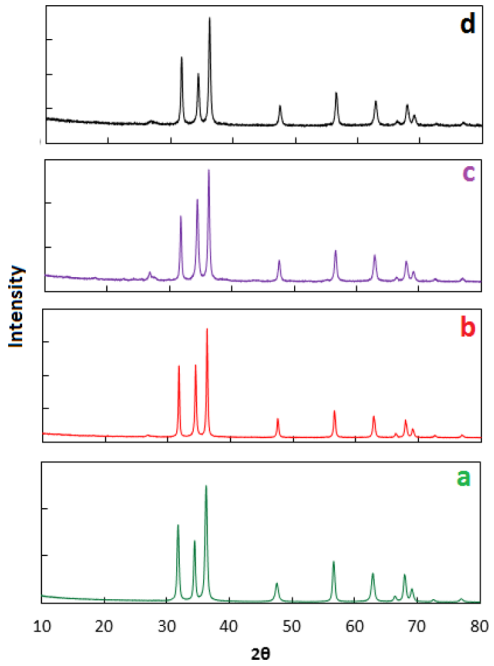

Figure 1. XRD pattern of ZnO (a), 5% Co−ZnO (b), 10% Co−ZnO (c), and 15% Co−ZnO (d).

match to standard diffraction data for ZnO, as expected. The XRD patterns exhibit sharp peaks at 2θ degrees 34.43, 36.27, 47.55, 56.62, 62.88, 67.97, 68.11, 72.59, and 76.99 indexed to (0 0 2), (1 0 1), (1 0 2), (1 1 0), (1 0 3), (1 1 2), (2 0 1), (0 0 4), and (2 0 2) hkl crystal planes of ZnO, respectively (JCPDS card no. 89-0510).[27,28] It is reported that cobalt oxide shows a sharp peak at $2\theta \sim 36°$; however, it cannot be observed in the given XRD patterns due to the low concentration of Co.[29] The enlarged view of XRD given in Figure 2 shows that peak intense position of 5% Co−ZnO, 10% Co−ZnO, and 15% Co−ZnO is offset by 0.07, 0.12, and 0.16, respectively, compared to a peak position of ZnO. This shift in peak position shows that Co^{2+} has been doped in ZnO.[30]

3.2. X-ray Photoelectron Spectroscopy. XPS analysis for the ZnO and Co−ZnO was conducted to find out the chemical states and elemental compositions. The XPS spectra given in Figure 3 exhibit peaks for Zn, Co, and O which confirm the existence of three elements in the as-prepared Co−ZnO photocatalyst. Figure 3a shows the Zn 2p core-level spectra for ZnO and Co−ZnO samples. The Zn 2p spectra

https://dx.doi.org/10.1021/acsomega.0c05092
ACS Omega 2021, 6, 1426−1435

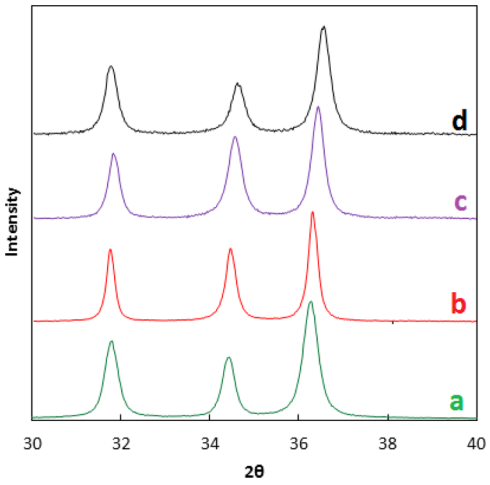

Figure 2. Enlarged view of XRD pattern of ZnO (a), 5% Co−ZnO (b), 10% Co−ZnO (c), and 15% Co−ZnO (d).

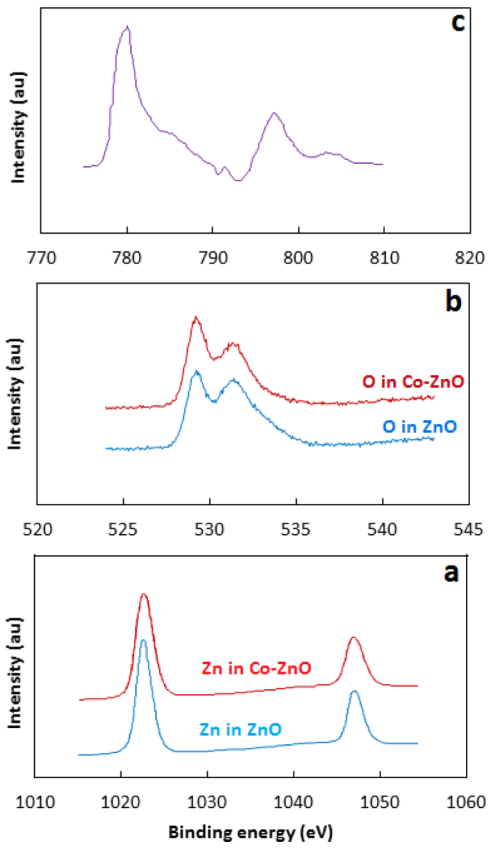

Figure 3. XPS spectra of Zn 2p (a) O 1s (b) and Co 2p (c).

exhibit two peaks at binding energy ∼ 1022 and ∼1047 eV attributed to the Zn $2p_{3/2}$ and Zn $2p_{1/2}$, respectively. Moreover, the positions of the peaks in Co−ZnO slightly shifted to higher binding energy (peak for Zn $2p_{3/s}$ shifted from 1022.64 to 1022.76 eV; the peak for Zn $2p_{1/2}$ shifted from 1047.14 to 1047.26 eV) compared to ZnO. This may be due to the less concentration of Zn in the Co−ZnO sample as compared to ZnO.[31,32] Figure 3b shows the O 1s core-level spectra of the ZnO and Co−ZnO. The O 1s core-level spectra exhibit two peaks at binding energies 529.3 and 531.5 eV which represent lattice oxygen (O_L) and chemisorbed oxygen (O_H), respectively. The lower energy peak in O 1s spectra is attributed to the intrinsic O^{2-} ions in the wurtzite structure of the hexagonal Zn^{2+} ion array, while the higher energy peak is attributed to O^{2-} ions in the oxygen-deficient area of ZnO.[33,34] Figure 3c shows the Co 2p spectrum of Co−ZnO which exhibits two peaks, one at 780.3 eV and the other 795.8 eV. These peaks are attributed to Co 2p3/2 and Co 2p1/2, respectively. The difference in the binding energy of Co 2p1/2 and Co 2p3/2 is 15.5 eV, which matches that of standard CoO. These results show that Co exists in a high-spin divalent state of Co, Co^{2+}, in ZnO.[35,36]

3.3. UV−Visible Diffuse Reflectance Spectroscopy. The effectiveness of Co−ZnO as a photocatalyst for photodegradation of organic pollutants under visible irradiation by reducing the band gap energy can be confirmed by the analysis of UV−visible diffuse reflectance spectroscopy (UV−vis DRS) spectra. Figure 4 reflects the UV−vis DRS spectra of ZnO and

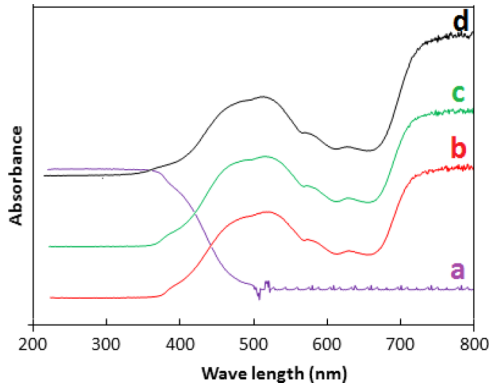

Figure 4. DRS UV/vis spectrum of ZnO (a) 5% Co−ZnO (b) 10% Co−ZnO (c) 15% Co−ZnO (d).

Co−ZnO samples which show that implantation of Co influences the absorption capability of light. As XRD and XPS results confirm the formation of Co-doped ZnO, therefore, dramatically different UV−vis DRS spectra of Co−ZnO samples compared to pure ZnO are expected. The UV−vis spectra of Co−ZnO samples show that the absorption edges move to a longer wavelength thus showing a redshift. This redshift has been attributed to defect centers created due to Co^{2+} that may lead to lattice strain. The estimated band gap energy for ZnO is 3.37 eV, whereas for the cobalt-doped ZnO composite is 2.16 eV which shows that doping of Co narrows the band gap of Co−ZnO. Hence, Co−ZnO can be used as an effective catalyst for photodegradation of organic pollutants under visible irradiation.[37−39]

3.4. PEC Measurements. PEC measurement experiments using the CO_2 bubbled system were conducted to evaluate the photocatalytic efficiency of ZnO and Co−ZnO. Figure 5 shows the results of PEC analyses. It was observed that the reduction current is greater for Co−ZnO as compared to ZnO in the CO_2 bubbled system. It suggests the superiority of catalytic performance of Co−ZnO compared to ZnO due to the appropriate ionic radius of Zn and surface basicity of ZnO. ZnO can act as a good platform for accepting high-energy photoelectrons from Co to enhance the charge separation resulting a good photocatalytic efficiency under visible irradiation and maintaining the thermodynamic energy.[40,41]

3.5. Temperature-Programmed Desorption. For a good photocatalyst, the surface adsorption and activation of the O_2 is an eminent step to lower the recombination of

https://dx.doi.org/10.1021/acsomega.0c05092
ACS Omega 2021, 6, 1426−1435

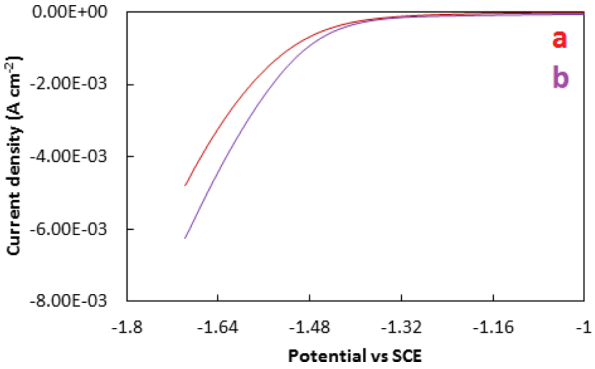

Figure 5. Electrochemical reduction curves of ZnO (a) and Co−ZnO (b) in the CO_2 bubbled system.

photogenerated electrons in the conduction band and photoinduced positive holes in the valence band resulting in the improvement of charge separation. As the recombination is lowered and charge separation is enhanced, the photocatalytic efficiency of the photocatalyst for the degradation of organic pollutants is enhanced.[42] For the determination of adsorption capacity of O_2 of the ZnO and Co−ZnO, oxygen TPD (O_2-TPD), curves of ZnO and Co−ZnO were obtained and analyzed as given in Figure 6. Three kinds of desorption peaks

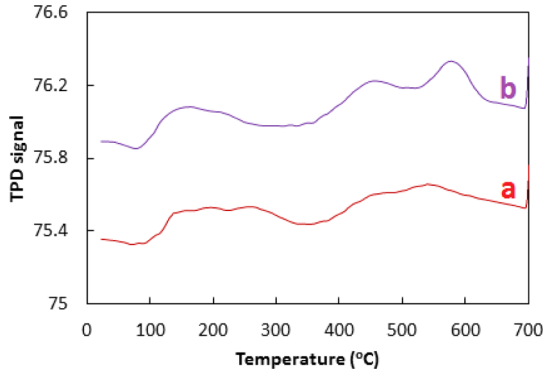

Figure 6. O_2 TPD (O_2-TPD) analysis for ZnO (a) and Co−ZnO (b).

were observed at 100−600 °C in O_2-TPD which can be attributed to the physical adsorption of O_2 at low temperatures and chemical adsorption of O_2 at high temperatures. The peak at 300−450 °C in O_2-TPD showed the desorption of O_2 on ZnO. Also, a peak above 500 °C depicted the desorption of O_2 on Co particles. O_2-TPD signals were found stronger in the case of Co−ZnO which indicated the greater adsorption of O_2 which lowered the recombination of the photogenerated electron and photoinduced positive hole and enhanced the charge separation leading to the improvement in the photocatalytic efficiency of the photocatalyst.[43]

3.6. PL Spectroscopy. PL spectra of ZnO and Co−ZnO are given in Figure 7. The PL spectra exhibit a UV near-band-edge emission peak around 380 nm and blue-green emission with 485 nm wavelength. The emission peak at ∼380 nm is known to be caused by the band-to-band transition of excitons while the peak at 485 nm originates from the electron transition from the level of the ionized oxygen vacancies to the valence band.[44] The emission peak at ∼380 nm is due to the band edge emission by radiative annihilation of excitons. It is related to the recombination of free and shallow bound excitons.[45,46] The emission peak at 485 nm may also be

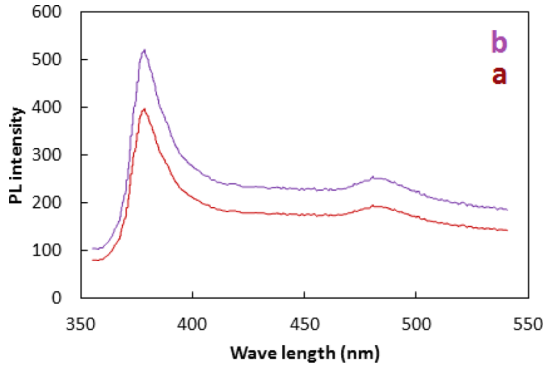

Figure 7. PL spectra of ZnO (a) and Co−ZnO (b).

attributed to the formation of the surface defect (SD) and the formation of hydroxyl radicals. The PL spectra of both ZnO and Co−ZnO have the same characteristics; however, the intensity of the PL spectrum of Co−ZnO is higher compared to the intensity of ZnO. It has been reported that Co−ZnO behaves as a quenching center to inhibit the recombination of exciton due to electron transfer processes from donor−acceptor pairs to neighboring Co ions in the ZnO lattice.[47] As a result, Co−ZnO may act as an efficient photocatalyst for the degradation of organic pollutants.

3.7. Fluorescence Spectroscopy related to OH• Measurements. As the formation of OH radicals is involved in photocatalysis, therefore, the amount of OH radicals produced was evaluated by the Coumarin fluorescent method. In this method, Coumarin is used as it produces easily luminescent 7-hydroxy coumarin by reaction with OH radicals. Generally, the higher is the amount of OH radicals, the stronger will be the intensity of fluorescent signals in the fluorescent spectrum. Figure 8 shows the fluorescence spectra

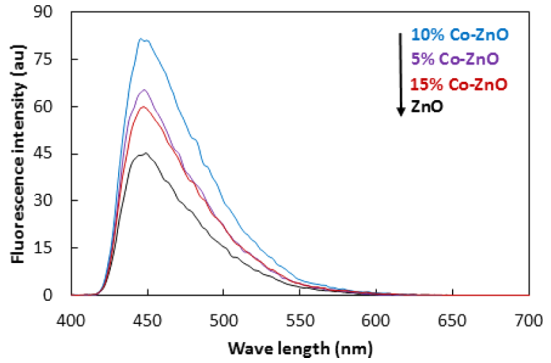

Figure 8. Fluorescent spectra related to OH radicals.

related to the produced OH of ZnO and Co−ZnO composites. It can be seen that the OH radical fluorescent intensity of Co−ZnO is stronger than that of pure ZnO with the increasing amount of Co coupling, especially in the case of a 10% Co−ZnO sample. Conversely, if the quantities of used Co-doped ZnO are in excess, the number of hydroxyl radicals (OH•) generated starts to decrease which may be due to the low charge separation. Hence, 10% Co−ZnO is considered an efficient photocatalyst for photodegradation of organic pollutants.[40]

3.8. Photocatalytic Activity. To find the latent catalytic applications of the as-prepared Co−ZnO composites in the remediation of environmental pollution, we have studied the

https://dx.doi.org/10.1021/acsomega.0c05092
ACS Omega 2021, 6, 1426−1435

photocatalytic degradation of the methyl orange dye as a model pollutant over Co−ZnO as a photocatalyst under visible irradiation. In a typical experiment, a 50 mL of solution of methyl orange with an initial concentration of 100 mg/L was treated at 30 °C with 0.05 g of catalyst under visible irradiation for 120 min using a Pyrex glass beaker as a batch reactor. Before visible irradiation, the reaction mixture composed of methyl orange solution, and the catalyst was stirred for 30 min under dark conditions. Similarly, the dye solution was stirred and irradiated in the absence of a catalyst for 30 min as a blank reaction. The photocatalytic degradation was monitored by a UV−vis spectrophotometer. Figure 9 shows the photocatalytic

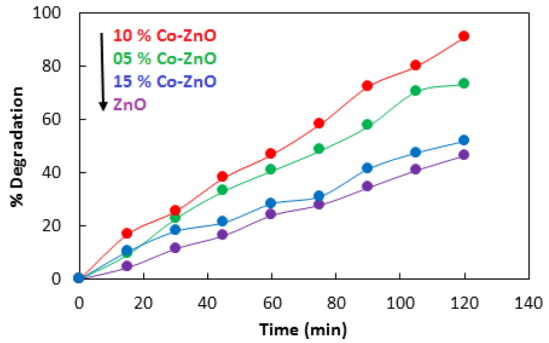

Figure 9. Photodegradation of methyl orange with ZnO, 5% Co−ZnO, 10% Co−ZnO, and 15% Co−ZnO.

activity of ZnO, 5% Co−ZnO, 10% Co−ZnO, and 15% Co−ZnO toward photodegradation of methyl orange. Data given in Figure 9 illustrates that 10% Co−ZnO showed the highest photocatalytic activity with 93% degradation of methyl orange compared to 73, 52, and 46% with 5% Co−ZnO, 15% Co−ZnO, and ZnO, respectively. Hence, the implantation of Co enhances the photocatalytic activity of ZnO toward photodegradation of methyl orange. The DR UV−vis spectroscopy and fluorescence spectroscopy related to $\dot{O}H$ measurements also have suggested the enhanced photocatalytic activity of Co−ZnO as compared to ZnO. However, 15% Co−ZnO showed comparatively less catalytic activity. This was arisen due to the bulkiness of the composite because of the presence of cobalt on ZnO. Higher loading of cobalt covered the active sites which were necessary for the accumulation of the dye molecule and hence lowered the removal percentage of dye from the solution.

The recycling of catalysts is very important for sustainable wastewater treatment. Therefore, it is necessary to confirm whether Co−ZnO can be recycled in the photodegradation of methyl orange or not. For this purpose, 10% Co−ZnO was reused three times for photodegradation of methyl orange. The spent catalyst was reused after thorough washing with ethanol and distilled water followed by drying. It was observed that Co−ZnO exhibited nearly the same photocatalytic activity in each cycle.

The photocatalytic activity of Co−ZnO for photodegradation of methyl orange is compared with different heterostructures reported as photocatalysts for degradation of methyl orange. The data given in Table 1 shows that the photocatalyst reported in this study is more effective toward photodegradation of methyl orange as compared to already reported catalysts.

3.9. Mechanism and Kinetics. Based on analyses of UV−vis DRS and PL spectroscopy, it is suggested that implantation

Table 1. Semiconductor−Semiconductor Heterostructures Reported as Catalysts for Photodegradation of Methyl Orange

no	heterostructure (g)	MO (mg/L)	efficiency (%)	refs
1	TiO_2−BiOBr (0.2)	10	90	Wang et al., 2015[48]
2	TiO_2−MoS_2 (0.05)	20	97	Zhang et al., 2015[49]
3	Ag_2O−Ag_3PO_4 (0.05)	50	100	Wang et al., 2013[50]
4	SnO_X−Zn_2SnO_4 (0.1)	20	83	Wang et al., 2017[51]
5	C_3N_4−$Bi_5Nb_3O_{15}$ (0.1)	15	94	Zhang et al., 2013[52]
6	SnS_2−TiO_2 (0.1)	2	92	Dai et al., 2018[53]
7	β-Bi_2O_3-α-Bi_2O_3 (0.2)	4	95	Hou et al., 2013[54]
8	Bi_2O_3−BiOI (0.1)	2	95	Han et al., 2015[55]
9	BiOI−BiOBr (0.1)	10	63	Cao et al., 2011[56]
10	TiO_2-β-anatase (0.02)	5	100	Zhang et al., 2013[57]
11	$In_{2.77}$−S_4−$SrCO_3$ (0.02)	5	100	Wu et al., 2018[58]
12	ZrO_2−MoS_2 (0.05)	10	95	Prabhakar Vattikuti et al., 2016[59]
13	$Bi1_2TiO_{20}$-g-$C3N_4$ (0.2)	20	90	Cao et al., 2019[60]
14	Bi_2MoO_6−Bi_5O_7Br−TiO_2 (0.2)	16	47	Wang et al., 2020[61]
15	WO_3-g-C_3N_4 (0.1)	10	93	Yan et al., 2019[62]
16	$LaNiO_3/TiO_2$ (0.1)	20	92	Chen et al., 2020[63]
17	$ZnFe_2O_4$−SnS_2 (0.1)	50	99	Zhou et al., 2020[64]
18	$Ag_2Mo_{1-x}W_xO_4$ (0.05)	5	45	Andrade Neto et al., 2020[65]
19	Co_3O_4-g-C_3N_4 (0.1)	10	99	Han et al., 2014[66]
20	Co−ZnO (0.05)	100	93	this study
		200	60	
		300	54	

of Co creates SDs in ZnO. These SDs enhance the photocatalytic activity of ZnO toward the photodegradation of methyl orange. It is well known that irradiation of photocatalysts induces the formation of the exciton (pair of hole and electron) in valence and conduction bands. The SDs trap the positive hole induced in the valence band and produce surface-active centers (SD*). Then, an adduct species (SD/MO) is formed by the reaction of the surface-active center with methyl orange. Finally, the adduct species decompose and give the final degradation products. Similarly, the electrons induced in the conduction band react with oxygen adsorbed at Co−ZnO and produce superoxide anion radicals which finally produce the OH radical by series of reactions. The OH radicals degrade the methyl orange molecules.[67,68]

The whole process can be outlined as

$$\text{Co} - \text{ZnO} + h\nu \rightarrow h_{\text{Co-ZnO}}^{+} + e_{\text{Co-ZnO}}^{-} \quad (1)$$

$$\text{SD} + h_{\text{Co-ZnO}}^{+} \rightarrow \text{SD}^* \quad (2)$$

$$\text{SD}^* + \text{MO} \rightarrow \text{SD: MO} \quad (3)$$

https://dx.doi.org/10.1021/acsomega.0c05092
ACS Omega 2021, 6, 1426−1435

$$\text{SD: MO} \rightarrow \text{SD} + \text{Degradation products} \quad (4)$$

$$e_{\text{Co-ZnO}}^{-} + (O_2)_{ads} \rightarrow \rightarrow \text{OH} \quad (5)$$

$$\text{OH} + \text{MO} \rightarrow \text{Degradation products} \quad (6)$$

Based on the above-mentioned reactions, the rate of reaction can be written as

$$-\frac{d[MO]}{dt} = \gamma_1[SD^*][MO] + \gamma_2[OH][MO] \quad (7)$$

$$-\frac{d[MO]}{dt} = (\gamma_1[SD^*] + \gamma_2[OH])[MO] \quad (8)$$

The above-mentioned rate expression represents a typical Eley−Rideal mechanism. Under continuous irradiation of a reaction mixture containing a fixed amount of catalyst, the rate of reaction becomes independent on SD and exciton; hence, the rate expression can be written as expression 9 (k_{obs} = observed rate constant, n = order of reaction concerning methyl orange).

$$-\frac{d[MO]}{dt} = k_{obs}[MO]^n \quad (9)$$

Rate expression 9 changes to expression 10 and 11 for $n = 1$ and $n = 2$, respectively (k_1 = first apparent order rate constant, k_2 = second order apparent rate constant).

$$\ln\frac{[MO]_0}{[MO]_t} = k_1 t \quad (10)$$

$$\frac{1}{[MO]_t} = k_2 t + \frac{1}{[MO]_0} \quad (11)$$

For reaction kinetics, the data given in Figure 9 was treated according to first-order kinetics (eq 10) and second-order kinetics (eq 11). Figure 10 shows the treatment of degradation data according to given kinetics models. Table 2 shows the measured rate constants. Based on a comparison of regression coefficients, R^2, it is suggested that photodegradation of methyl orange follows the first-order kinetics.

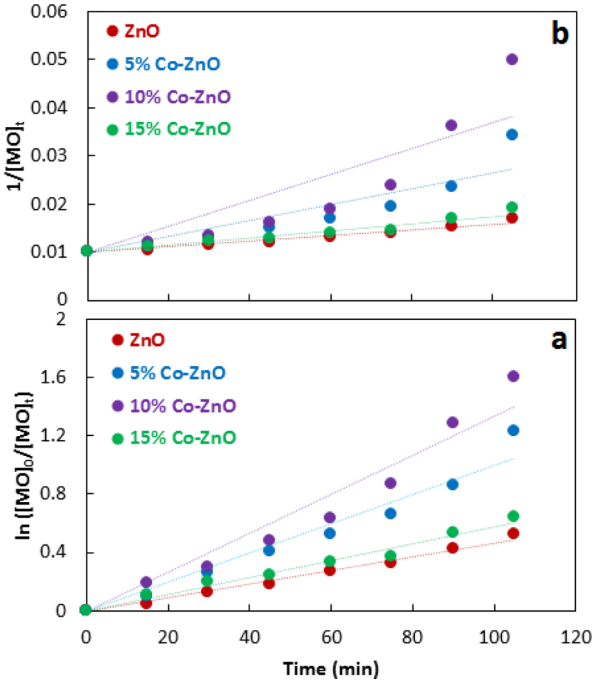

Figure 10. Treatment of photodegradation data of methyl orange according to 1st (a) and 2nd (b) order kinetics.

Table 2. Kinetics Parameters Determined by Treatment of Photodegradation Data of Methyl Orange According to 1st and 2nd Order Kinetics

	1st order kinetics		2nd order kinetics	
catalyst	k_1	R^2	k_2	R^2
ZnO	0.005	0.98	0.00006	0.91
5% Co−ZnO	0.01	0.95	0.0002	0.82
10% Co−ZnO	0.014	0.95	0.0003	0.78
15% Co−ZnO	0.006	0.98	0.00005	0.91

3.10. Effect of the Catalyst Dose. The optimization of the amount of catalyst is essential to avoid the unnecessary use of photocatalysts in the photocatalytic experiments. The catalyst dose was optimized by performing photodegradation experiments of methyl orange over 0.01−0.15 g of catalyst for 120 min. Figure 11 shows the results of photodegradation of

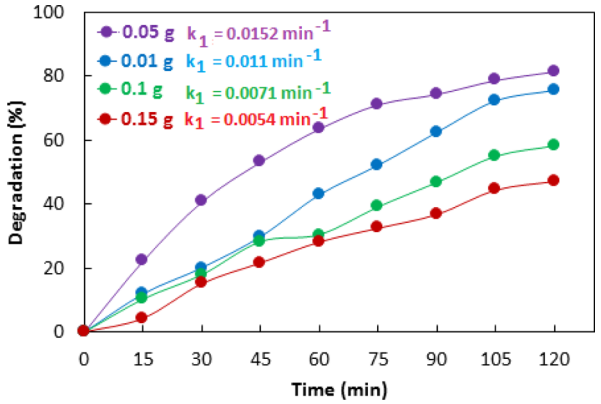

Figure 11. Effect of the catalyst dose on photodegradation and the first-order apparent rate constant of methyl orange catalyzed by 10% Co−ZnO.

100 mg/L methyl orange over different dose of 10% Co−ZnO catalyst. It was observed that photodegradation of methyl orange increased with the catalyst dose from 0.01 to 0.05 g and decreased with a further increase in the catalyst dose. Similarly, the rate constant observed with 0.05 g of catalyst was higher than the rate constants observed with other dosages as given in Figure 11. The number of active centers increases with the catalyst dose which increases the catalytic activity. However, the reaction mixture with an increased catalyst dose cannot be homogenized properly at a given speed of agitation; therefore, the active centers become nonaccessible with a higher catalyst dose resulting in decreased catalytic activity. Furthermore, the higher catalyst dose inhibits the penetration of irradiation to the interior of the solution, which ultimately causes a retardation effect on catalytic activity.[69]

3.11. Effect of pH. As pH of the reaction mixture affects the production of OH radicals, the adsorption of methyl orange on the catalyst surface, and the charges on the surface of the catalyst, therefore, the pH dependence of photodegradation of methyl orange catalyzed by Co−ZnO was investigated. For this purpose, photodegradation experiments

https://dx.doi.org/10.1021/acsomega.0c05092
ACS Omega 2021, 6, 1426−1435

with 0.05 g of Co−ZnO catalyst and 100 mg/L solution of methyl orange were conducted over pH range 2−10. For adjustment of pH, 0.1 M NaOH and 0.1 M HCl were used. As given in Figure 12, the highest photodegradation of methyl

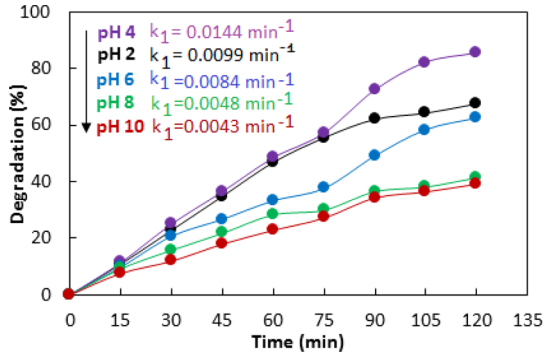

Figure 12. Effect of pH on photodegradation and first-order apparent rate constant (inset) of methyl orange catalyzed by 10% Co−ZnO.

orange achieved at pH 4. The observed rate constants were determined as 0.0099, 0.0144, 0.0084, 0.0048, and 0.0043 per minute at pH 2, 4, 6, 8, and 10, respectively. The pH of point of zero charge (pHpzc) for ZnO has been reported in the range 6.9−9.8.[70,71] The pH above PZC makes the surface of ZnO positive while pH below PZC makes the surface of ZnO negative. The positively charged surface at acidic pH is expected as conductive for the transfer of electrons to the catalyst surface where the reduction of oxygen to the superoxide anion radical is initiated. The superoxide anion radicals yield OH radicals resulting in enhanced photocatalytic activity. Furthermore, methyl orange exists in the anionic form at acidic pH; therefore, the lower pH favors the adsorption of the anionic methyl orange dye on the surface of positively charged ZnO due to electrostatic interaction, resulting in an enhanced photocatalytic activity at lower pH. However, the strongly acidic solution causes the dissolution of ZnO; therefore, pH lower than 4 caused a decrease in photocatalytic activity. On the other hand, the photocatalytic activity of Co−ZnO decreased at higher pH due to electrostatic repulsion between the negatively charged catalyst and anionic methyl orange dyes.[72]

3.12. Effect of Temperature. As temperature significantly affects the rate of reaction, therefore, the dependence of the rate of reaction on the temperature was also evaluated by conducting photodegradation experiments with 0.05 g of 10% Co−ZnO/50 mL of 100 mg/L methyl orange at 30, 40, and 50 °C separately. Figure 13a shows that photocatalytic activity increases with temperature. Figure 13b shows the kinetics treatment of degradation data which shows that the rate constant increases with temperature. The temperature dependence of the rate was further investigated using the Arrhenius equation (eq 12) and the Eyring equation (eq 13). Figure 14 shows the analyses of rate constants according to Arrhenius and Eyring equations. The energy of activation (E) was calculated from the Arrhenius plot as 15.1 kJ/mol. The enthalpy (ΔH) and entropy (ΔS) was calculated from the Eyring plot as 12.5 kJ/mol and 241.1 J/mol, respectively. The free energy of reaction (ΔG) was calculated as −62.9 kJ/mol indicating the spontaneity of reaction. Although the photochemical reactions do not depend on the temperature, however, the variation of rate constants with temperature

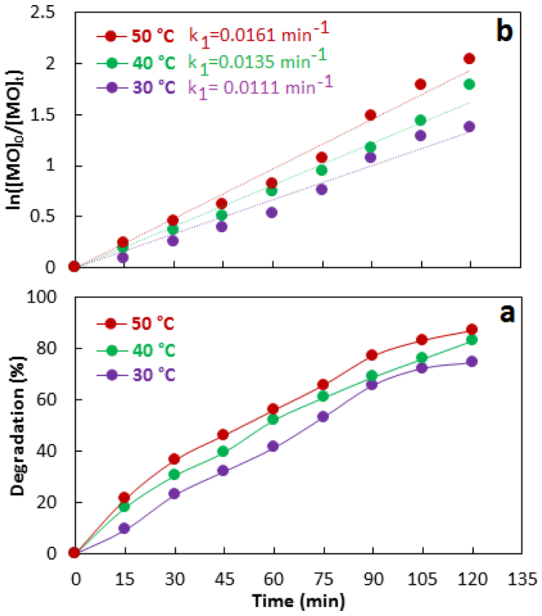

Figure 13. Effect of temperature on 10% Co−ZnO catalyzed photodegradation of methyl orange (b), treatment of photodegradation data according to the first-order kinetics model (b).

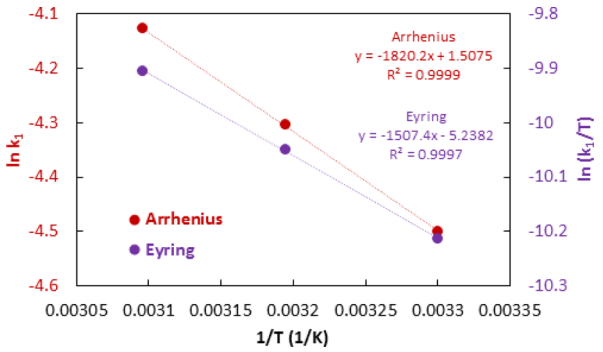

Figure 14. Effect of temperature on Co−ZnO catalyzed photodegradation of methyl orange in terms of the Arrhenius and Eyring plot.

and the existence of activation energy in this study show that thermal activation is an important step for accelerating the diffusion of methyl orange to the Co−ZnO catalyst.

$$\ln k_1 = \ln A - \frac{E}{RT} \tag{12}$$

$$\ln \frac{k_1}{T} = \ln \frac{k_b}{h} + \frac{\Delta S}{R} - \frac{\Delta H}{RT} \tag{13}$$

3.13. Effect of Concentration. Considering the practical application, the dye concentration dependence of photocatalytic activity toward the degradation of dyes is very important. Therefore, the dependence of the photocatalytic activity of 10% Co−ZnO for degradation of methyl orange was investigated in 100−400 mg/L initial dye concentration in the presence of 0.05 g/50 mL catalyst at 30 °C. As shown in Figure 15, the photocatalytic activity of 10% Co−ZnO decreased with an increase in the concentration of methyl orange. At higher dye concentrations, the photons cannot penetrate to the surface of the catalyst due to absorption by dye molecules. Additionally, a higher concentration of dye

https://dx.doi.org/10.1021/acsomega.0c05092
ACS Omega 2021, 6, 1426−1435

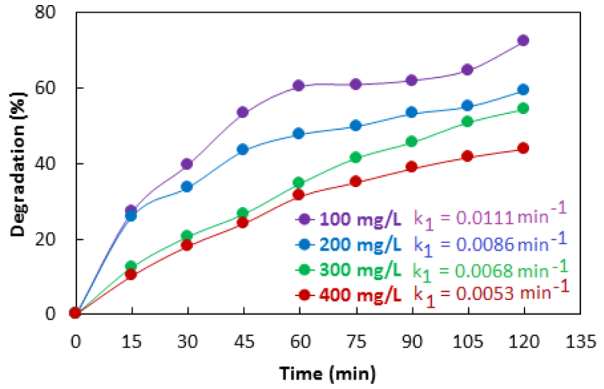

Figure 15. Concentration dependence of 10% Co−ZnO catalyzed photo degradation of methyl orange.

favors the adsorption of the dye on the surface of Co−ZnO. These two factors decrease the yield of exciton and OH radicals and ultimately cause a decreasing effect on photocatalytic activity at the higher concentration.[16,71,72]

4. CONCLUSIONS

Herein, we reported the synthesis and characterization of ZnO and Co−ZnO as photocatalysts for the photodegradation of methyl orange. The implantation of Co on ZnO was confirmed by XRD, XPS, and DR-UV−vis spectroscopy. The photocatalytic degradation of methyl orange showed that implantation of 10% Co significantly enhanced the photocatalytic activity of ZnO. The effect of experimental parameters including recycling of the catalyst, catalyst dosage, pH, temperature, and dye concentration on photocatalytic activity was investigated. The reaction kinetics was investigated by treatment of degradation data according to the Eley-Rideal mechanism.

AUTHOR INFORMATION

Corresponding Author

Muhammad Saeed − *Department of Chemistry, Government College University Faisalabad, Faisalabad 38000, Pakistan;* orcid.org/0000-0002-8759-6948; Phone: +92 346 9010903; Email: msaeed@gcuf.edu.pk

Authors

Muhammad Adeel − *Department of Chemistry, Government College University Faisalabad, Faisalabad 38000, Pakistan*

Iltaf Khan − *College of Chemical and Materials Engineering, Beijing Institute of Petrochemical Technology, Beijing 102617, China*

Majid Muneer − *Department of Chemistry, Government College University Faisalabad, Faisalabad 38000, Pakistan*

Nadia Akram − *Department of Chemistry, Government College University Faisalabad, Faisalabad 38000, Pakistan*

Complete contact information is available at: https://pubs.acs.org/10.1021/acsomega.0c05092

Notes

The authors declare no competing financial interest.

ACKNOWLEDGMENTS

Financial support of Government College University Faisalabad Pakistan under GCUF-RSP is gratefully acknowledged.

REFERENCES

(1) Vallejo, W.; Cantillo, A.; Salazar, B.; Diaz-Uribe, C.; Ramos, W.; Romero, E.; Hurtado, M. Comparative Study of ZnO Thin Films Doped with Transition Metals (Cu and Co) for Methylene Blue Photodegradation under Visible Irradiation. *Catalysts* **2020**, *10*, 528.

(2) Lellis, B.; Fávaro-Polonio, C. Z.; Pamphile, J. A.; Polonio, J. C. Effects of Textile Dyes on Health and the Environment and Bioremediation Potential of Living Organisms. *Biotechnol. Res. Innov.* **2019**, *3*, 275−290.

(3) Hassan, M. M.; Carr, C. M. A Critical Review on Recent Advancements of the Removal of Reactive Dyes from Adsorbents, Dyehouse Effluent by Ion-Exchange. *Chemosphere* **2018**, *209*, 201−219.

(4) Julkapli, N. M.; Bagheri, S.; Bee Abd Hamid, S. Recent Advances in Heterogeneous Photocatalytic Decolorization of Synthetic Dyes. *Sci. World J.* **2014**, *2014*, 692307.

(5) Daij, K. B.; Bellebia, S.; Bengharez, Z. Comparative Experimental Study On The Cod Removal In Aqueous Solution Of Pesticides By The Electrocoagulation Process Using Monopolar Iron Electrodes. *Chem. Int.* **2017**, *3*, 420−427.

(6) Djehaf, K.; Bouyakoub, A. Z.; Ouhib, R.; Benmansour, H.; Bentouaf, A.; Mahdad, A.; Moulay, N.; Bensaid, D.; Ameri, M. Textile Wastewater in Tlemcen (Western Algeria): Impact, Treatment by Combined Process. *Chem. Int.* **2017**, *3*, 414−419.

(7) Minas, F.; Chandravanshi, B. S.; Leta, S. Chemical Precipitation Method for Chromium Removal and Its Recovery from Tannery Wastewater in Ethiopia. *Chem. Int.* **2017**, *3*, 392−405.

(8) Ayach, A.; Fakhil, S.; Faiz, Z.; Bouih, A.; Malek, O. A.; Benkdad, A.; Benmansour, M.; Laissaoui, A.; Adjour, M.; Elbatal, Y.; Vioque, I.; Manjon, G. Adsorption of Methylene Blue on Bituminous Schists from Tarfaya-Boujdour. *Chem. Int.* **2017**, *3*, 442−451.

(9) Jafarinejad, S. Activated Sludge Combined with Powdered Activated Carbon (PACT Process) for the Petroleum Industry Wastewater Treatment: A Review. *Chem. Int.* **2017**, *3*, 368−374.

(10) Chen, R. X.; Zhu, S. L.; Mao, J.; Cui, Z. D.; Yang, X. J.; Liang, Y. Q.; Li, Z. Y. Synthesis of CuO/Co_3O_4 Coaxial Heterostructures for Efficient and Recycling Photodegradation. *Int. J. Photoenergy* **2015**, *2015*, 183468.

(11) Manikandan, A.; Manikandan, E.; Meenatchi, B.; Vadivel, S.; Jaganathan, S. K.; Ladchumananandasivam, R.; Henini, M.; Maaza, M.; Aanand, J. S. Rare Earth Element (REE) Lanthanum Doped Zinc Oxide (La: ZnO) Nanomaterials: Synthesis Structural Optical and Antibacterial Studies. *J. Alloys Compd.* **2017**, *723*, 1155−1161.

(12) Chandekar, K. V.; Shkir, M.; Al-Shehri, B. M.; AlFaify, S.; Halor, R. G.; Khan, A.; Al-Namshah, K. S.; Hamdy, M. S. Visible Light Sensitive Cu Doped ZnO: Facile Synthesis, Characterization and High Photocatalytic Response. *Mater. Charact.* **2020**, *165*, 110387.

(13) Nisar, A.; Saeed, M.; Usman, M.; Muneer, M.; Adeel, M.; Khan, I.; Akhtar, J. Kinetic Modeling of ZnO-RGO Catalyzed Degradation of Methylene Blue. *Int. J. Chem. Kinet.* **2020**, *52*, 645.

(14) Saeed, M.; Adeel, S.; Abdur-Raoof, H.; Usman, M.; Mansha, A.; Ahmad, A.; Amjed, M. ZnO Catalyzed Degradation of Methyl Orange in Aqueous Medium. *Chiang Mai J. Sci.* **2017**, *44*, 1646−1653.

(15) Nair, M. G.; Nirmala, M.; Rekha, K.; Anukaliani, A. Structural, Optical, Photo Catalytic and Antibacterial Activity of ZnO and Co Doped ZnO Nanoparticles. *Mater. Lett.* **2011**, *65*, 1797−1800.

(16) Saeed, M.; Siddique, M.; Ibrahim, M.; Akram, N.; Usman, M.; Aleem, M. A.; Baig, A. Calotropis Gigantea Leaves Assisted Biosynthesis of ZnO and Ag@ZnO Catalysts for Degradation of Rhodamine B Dye in Aqueous Medium. *Environ. Prog. Sustain. Energy* **2020**, *39*, No. e13408.

(17) Ahmed, S. N.; Haider, W. Heterogeneous Photocatalysis and Its Potential Applications in Water and Wastewater Treatment: A Review. *Nanotechnology* **2018**, *29*, 342001.

(18) Khalid, N. R.; Ahmed, E.; Hong, Z.; Zhang, Y.; Ahmad, M. Nitrogen Doped TiO2 Nanoparticles Decorated on Graphene Sheets for Photocatalysis Applications. *Curr Appl Phys* **2012**, *12*, 1485−1492.

(19) Shkir, M.; Chandekar, K. V.; Alshehri, B. M.; Khan, A.; AlFaify, S.; Hamdy, M. S. A Remarkable Enhancement in Photocatalytic Activity of Facilely Synthesized Terbium@Zinc Oxide Nanoparticles by Flash Combustion Route for Optoelectronic Applications. *Appl. Nanosci.* **2020**, *10*, 1811−1823.
(20) Shkir, M.; Al-Shehri, B. M.; Pachamuthu, M. P.; Khan, A.; Chandekar, K. V.; AlFaify, S. A Remarkable Improvement in Photocatalytic Activity of ZnO Nanoparticles through Sr Doping Synthesized by One Pot Flash Combustion Technique for Water Treatments. *Colloids Surf., A* **2020**, *587*, 124340.
(21) Chandekar, K. V.; Shkir, M.; Khan, A.; Al-Shehri, B. M.; Hamdy, M. S.; AlFaify, S.; El-Toni, M. A.; Aldalbahi, A.; Ansari, A. A.; Ghaithan, H. A Facile One-Pot Flash Combustion Synthesis of La@ ZnO Nanoparticles and Their Characterizations for Optoelectronic and Photocatalysis Applications. *J. Photochem. Photobiol., A* **2020**, *395*, 112465.
(22) Bomila, R.; Srinivasan, S.; Gunasekaran, S.; Manikandan, A. Enhanced Photocatalytic Degradation of Methylene Blue Dye, Opto-Magnetic and Antibacterial Behaviour of Pure and La-Doped ZnO Nanoparticles. *J. Supercond. Novel Magn.* **2018**, *31*, 855−864.
(23) Ullah, R.; Dutta, J. Photocatalytic Degradation of Organic Dyes with Manganesedoped ZnO Nanoparticles. *J. Hazard. Mater.* **2008**, *156*, 194−200.
(24) Wu, Y.; Lu, G.; Li, S. The Doping Effect of Bi on TiO2 for Photocatalytic Hydrogen Generation and Photodecolorization of Rhodamine B. *J. Phys. Chem. C* **2009**, *113*, 9950−9955.
(25) Yalçın, Y.; Kılıç, M.; Çinar, Z. Fe+3-Doped TiO2: A Combined Experimental and Computational Approach to the Evaluation of Visible Light Activity. *Appl. Catal., B* **2010**, *99*, 469−477.
(26) Colón, G.; Maicu, M.; Hidalgo, M. C.; Navío, J. A. Cu-Doped TiO2 Systems with Improved Photocatalytic Activity. *Appl. Catal., B* **2006**, *67*, 41−51.
(27) Adeleke, J. T.; Theivasanthi, T.; Thiruppathi, M.; Swaminathan, M.; Akomolafe, T.; Alabi, A. B. Photocatalytic Degradation of Methylene Blue by ZnO/NiFe2O4 Nanoparticles. *Appl. Surf. Sci.* **2018**, *455*, 195−200.
(28) Kang, K.-M.; Wang, Y.; Kim, M.; Park, H.-H. Study on Properties of Ga/F-Co-Doped ZnO Thin Films Prepared Using Atomic Layer Deposition. *Thin Solid Films* **2018**, *660*, 913−919.
(29) Saeed, M.; Muneer, M.; Mumtaz, N.; Siddique, M.; Akram, N.; Hamayun, M. Ag-Co3O4: Synthesis, Characterization and Evaluation of Its Photo-Catalytic Activity towards Degradation of Rhodamine B Dye in Aqueous Medium. *Chin. J. Chem. Eng.* **2018**, *26*, 1264−1269.
(30) Yang, Y.; Wang, X.; Yi, G.; Li, H.; Shi, C.; Sun, G.; Zhang, Z. Hydrothermal Synthesis of Co3 O4/Zno Hybrid Nanoparticles for Triethylamine Detection. *Nanomaterials* **2019**, *9*, 1599.
(31) Reddy, I. N.; Reddy, C. V.; Shim, J.; Akkinepally, B.; Cho, M.; Yoo, K.; Kim, D. Excellent Visible-Light Driven Photocatalyst of (Al, Ni) Co-Doped ZnO Structures for Organic Dye Degradation. *Catal. Today* **2020**, *340*, 277−285.
(32) Achouri, F.; Corbel, S.; Balan, L.; Mozet, K.; Girot, E.; Medjahdi, G.; Said, M. B.; Ghrabi, A.; Schneider, R. Porous Mn-Doped ZnO Nanoparticles for Enhanced Solar and Visible Light Photocatalysis. *Mater. Des.* **2016**, *101*, 309−316.
(33) Zhang, L.; Ye, Z.; Lu, B.; Lu, J.; Zhang, Y.; Zhu, L.; Huang, J.; Zhang, W.; Huang, J.; Zhang, J.; Jiang, J.; Wu, K.; Xie, Z. Ferromagnetism Induced by Donor-Related Defects in Co-Doped ZnO Thin Films. *J. Alloys Compd.* **2011**, *509*, 2149−2153.
(34) Kim, G. H.; Kim, D. L.; Ahn, B. D.; Lee, S. Y.; Kim, H. J. Investigation on Doping Behavior of Copper in ZnO Thin Film. *Microelectron. J.* **2009**, *40*, 272−275.
(35) Wang, C. C.; Liu, M.; Man, B. Y.; Chen, C. S.; Jiang, S. Z.; Yang, S. Y.; Gao, X. G.; Xu, S. C.; Hu, B.; Sun, Z. C. Effect of Oxygen Pressure on the Structural, Optical and Magnetic Properties of Pulsed Laser Ablated ZnCoO Thin Films. *J. Alloys Compd.* **2012**, *520*, 158−163.
(36) Cao, P.; Zhao, D. X.; Shen, D. Z.; Zhang, J. Y.; Zhang, Z. Z.; Bai, Y. Cu + -Codoping Inducing the Room-Temperature Magnetism and p-Type Conductivity of ZnCoO Diluted Magnetic Semiconductor. *Appl. Surf. Sci.* **2009**, *255*, 3639−3641.
(37) Chauhan, N.; Singh, V.; Kumar, S.; Sirohi, K.; Siwatch, S. Synthesis of Nitrogen- and Cobalt-Doped Rod-like Mesoporous ZnO Nanostructures to Study Their Photocatalytic Activity. *J. Sol-Gel Sci. Technol.* **2019**, *91*, 567−577.
(38) Mohamed, R. M.; McKinney, D.; Kadi, M. W.; Mkhalid, I. A.; Sigmund, W. Cobalt/Zinc Oxide Hollow Spheres: Visible Light Nanophotocatalysts. *Ceram. Int.* **2016**, *42*, 2299−2305.
(39) Kumar, Y.; Sahai, A.; Olive-Méndez, S. F.; Goswami, N.; Agarwal, V. Morphological Transformations in Cobalt Doped Zinc Oxide Nanostructures: Effect of Doping Concentration. *Ceram. Int.* **2016**, *42*, 5184−5194.
(40) Khan, I.; Sun, N.; Zhang, Z.; Li, Z.; Humayun, M.; Ali, S.; Qu, Y.; Jing, L. Improved Visible-Light Photoactivities of Porous LaFeO3 by Coupling with Nanosized Alkaline Earth Metal Oxides and Mechanism Insight. *Catal. Sci. Technol.* **2019**, *9*, 3149−3157.
(41) Khan, I.; Sun, N.; Wang, Y.; Li, Z.; Qu, Y.; Jing, L. Synthesis of SnO 2 / Yolk-Shell LaFeO 3 Nanocomposites as e Ffi Cient Visible-Light Photocatalysts for 2 , 4-Dichlorophenol Degradation. *Mater. Res. Bull.* **2020**, *127*, 110857.
(42) Saeed, M.; Siddique, M.; Usman, M.; Ul Haq, A.; Khan, S. G.; Raoof, H. A. Synthesis and Characterization of Zinc Oxide and Evaluation of Its Catalytic Activities for Oxidative Degradation of Rhodamine B Dye in Aqueous Medium. *Z. Phys. Chem.* **2017**, *231*, 1559−1572.
(43) Abdul-Kadhim, W.; Deraman, M. A.; Abdullah, S. B.; Tajuddin, S. N.; Yusoff, M. M.; Taufiq-Yap, Y. H.; Rahim, M. H. A. Efficient and Reusable Iron-Zinc Oxide Catalyst for Oxidative Desulfurization of Model Fuel. *J. Environ. Chem. Eng.* **2017**, *5*, 1645−1656.
(44) Lim, J.; Shin, K.; Wookim, H.; Lee, C. Photoluminescence Studies of ZnO Thin Films Grown by Atomic Layer Epitaxy. *J. Lumin.* **2004**, *109*, 181−185.
(45) Azmi, R.; Oh, S.-H.; Jang, S.-Y. High-Efficiency Colloidal Quantum Dot Photovoltaic Devices Using Chemically Modified Heterojunctions. *ACS Energy Lett.* **2016**, *1*, 100−106.
(46) Bouzourâa, M.-B.; Naciri, A. E.; Moadhen, A.; Rinnert, H.; Guendouz, M.; Battie, Y.; Chaillou, A.; Zaïbi, M.-A.; Oueslati, M. Effects of Silicon Porosity on Physical Properties of ZnO Films. *Mater. Chem. Phys.* **2016**, *175*, 233−240.
(47) Ravichandran, A. T.; Karthick, R. Enhanced Photoluminescence, Structural, Morphological and Antimicrobial Efficacy of Co-Doped ZnO Nanoparticles Prepared by Co-Precipitation Method. *Results Mater.* **2020**, *5*, 100072.
(48) Wang, X.-j.; Yang, W.-y.; Li, F.-t.; Zhao, J.; Liu, R.-h.; Liu, S.-j.; Li, B. Construction of Amorphous TiO2/BiOBr Heterojunctions via Facets Coupling for Enhanced Photocatalytic Activity. *J. Hazard. Mater.* **2015**, *292*, 126−136.
(49) Zhang, W.; Xiao, X.; Zheng, L.; Wan, C. Fabrication of TiO2/MoS2 Composite Photocatalyst and Its Photocatalytic Mechanism for Degradation of Methyl Orange under Visible Light. *Can. J. Chem. Eng.* **2015**, *93*, 1594−1602.
(50) Wang, P. Q.; Bai, Y.; Luo, P. Y.; Liu, J. Y. Ag2O/Ag3PO4 Heterostructures: Highly Efficient and Stable Visible-Light-Induced Photocatalyst for Degradation of Methyl Orange and Phenol. *Micro Nano Lett.* **2013**, *8*, 340−344.
(51) Wang, J.; Li, H.; Meng, S.; Zhang, L.; Fu, X.; Chen, S. One-Pot Hydrothermal Synthesis of Highly Efficient SnOx/Zn2SnO4 Composite Photocatalyst for the Degradation of Methyl Orange and Gaseous Benzene. *Appl. Catal., B* **2017**, *200*, 19−30.
(52) Zhang, S.; Yang, Y.; Guo, Y.; Guo, W.; Wang, M.; Guo, Y.; Huo, M. Preparation and Enhanced Visible-Light Photocatalytic Activity of Graphitic Carbon Nitride/Bismuth Niobate Heterojunctions. *J. Hazard. Mater.* **2013**, *261*, 235−245.
(53) Dai, G.; Qin, H.; Zhou, H.; Wang, W.; Luo, T. Template-Free Fabrication of Hierarchical Macro/Mesoporpous SnS 2 /TiO 2 Composite with Enhanced Photocatalytic Degradation of Methyl Orange (MO). *Appl. Surf. Sci.* **2018**, *430*, 488−495.

https://dx.doi.org/10.1021/acsomega.0c05092
ACS Omega 2021, 6, 1426−1435

(54) Hou, J.; Yang, C.; Wang, Z.; Zhou, W.; Jiao, S.; Zhu, H. In situ synthesis of α-β phase heterojunction on Bi2O3 nanowires with exceptional visible-light photocatalytic performance. *Appl. Catal., B* **2013**, *142*−*143*, 504−511.
(55) Han, S.; Li, J.; Yang, K.; Lin, J. Fabrication of a β-Bi2O3/BiOI Heterojunction and Its Efficient Photocatalysis for Organic Dye Removal. *Chin. J. Catal.* **2015**, *36*, 2119−2126.
(56) Cao, J.; Xu, B.; Luo, B.; Lin, H.; Chen, S. Novel BiOI/BiOBr Heterojunction Photocatalysts with Enhanced Visible Light Photocatalytic Properties. *Catal. Commun.* **2011**, *13*, 63−68.
(57) Zhang, Y.; Xu, J.; Feng, J.; Yang, A.; Liu, Y.; Zhi, M.; Hong, Z. Enhanced Photocatalytic Degradation of Methyl Orange in TiO 2(B) @anatase Heterostructure Nanocomposites Prepared by a Facile Hydrothermal Method. *Mater. Lett.* **2013**, *112*, 173−176.
(58) Wu, X.-F.; Li, H.; Sun, L.-S.; Su, J.-Z.; Zhang, J.-R.; Zhang, W.-G.; Zhang, M.; Sun, G.-W.; Zhan, L.; Zhang, M. One-Step Hydrothermal Synthesis of Visible-Light-Driven In2.77S4/SrCO3 Heterojunction with Efficient Photocatalytic Activity for Degradation of Methyl Orange and Tetracycline. *Appl. Phys. A: Mater. Sci. Process.* **2018**, *124*, 584.
(59) Prabhakar Vattikuti, S. V.; Byon, C.; Reddy, C. V. ZrO2/MoS2 Heterojunction Photocatalysts for Efficient Photocatalytic Degradation of Methyl Orange. *Electron. Mater. Lett.* **2016**, *12*, 812−823.
(60) Cao, L.; Li, Y.-F.; Tong, Y.; Yang, R.; Sun, L.; Cao, Q.; Chen, R. A Novel Bi12TiO20/g-C3N4 Hybrid Catalyst with a Bionic Granum Configuration for Enhanced Photocatalytic Degradation of Organic Pollutants. *J. Hazard. Mater.* **2019**, *379*, 120808.
(61) Wang, Y.; Wang, Q.; Zhang, H.; Wu, Y.; Jia, Y.; Jin, R.; Gao, S. CTAB-Assisted Solvothermal Construction of Hierarchical Bi2MoO6/Bi5O7Br with Improved Photocatalytic Performances. *Sep. Purif. Technol.* **2020**, *242*, 116775.
(62) Yan, H.; Zhu, Z.; Long, Y.; Li, W. Single-Source-Precursor-Assisted Synthesis of Porous WO3/g-C3N4 with Enhanced Photocatalytic Property. *Colloids Surf., A* **2019**, *582*, 123857.
(63) Chen, C.; Zhou, J.; Geng, J.; Bao, R.; Wang, Z.; Xia, J.; Li, H. Perovskite LaNiO3/TiO2 Step-Scheme Heterojunction with Enhanced Photocatalytic Activity. *Appl. Surf. Sci.* **2020**, *503*, 144287.
(64) Zhou, J.; Zhang, Z.; Kong, X.; He, F.; Zhao, R.; Wu, R.; Wei, T.; Wang, L.; Feng, J. A Novel P-N Heterojunction with Staggered Energy Level Based on ZnFe2O4 Decorating SnS2 Nanosheet for Efficient Photocatalytic Degradation. *Appl. Surf. Sci.* **2020**, *510*, 145442.
(65) Andrade Neto, N. F.; Lima, A. B.; Bomio, M. R. D.; Motta, F. V. Microwave-Assisted Hydrothermal Synthesis of Ag2Mo1-XWxO4 (x = 0, 0.25, 0.50, 0.75 and 1 Mol%) Heterostructures for Enhanced Photocatalytic Degradation of Organic Dyes. *J. Alloys Compd.* **2020**, *844*, 156077.
(66) Han, C.; Ge, L.; Chen, C.; Li, Y.; Xiao, X.; Zhang, Y.; Guo, L. Novel Visible Light Induced Co3O4-g-C3N4 Heterojunction Photocatalysts for Efficient Degradation of Methyl Orange. *Appl. Catal., B* **2014**, *147*, 546−553.
(67) Rauf, M. A.; Meetani, M. A.; Hisaindee, S. An Overview on the Photocatalytic Degradation of Azo Dyes in the Presence of TiO2 Doped with Selective Transition Metals. *Desalination* **2011**, *276*, 13−27.
(68) Pera-Titus, M.; García-Molina, V.; Baños, M. A.; Giménez, J.; Esplugas, S. Degradation of Chlorophenols by Means of Advanced Oxidation Processes: A General Review. *Appl. Catal., B* **2004**, *47*, 219−256.
(69) Muthirulan, P.; Nirmala Devi, C.; Meenakshi Sundaram, M. A Green Approach to the Fabrication of Titania-Graphene Nanocomposites: Insights Relevant to Efficient Photodegradation of Acid Orange 7 Dye under Solar Irradiation. *Mater. Sci. Semicond. Process.* **2014**, *25*, 219−230.
(70) Chen, C.; Liu, J.; Liu, P.; Yu, B. Investigation of Photocatalytic Degradation of Methyl Orange by Using Nano-Sized ZnO Catalysts. *Adv. Chem. Eng. Sci.* **2011**, *01*, 9−14.
(71) Chamjangali, M. A.; Boroumand, S. Synthesis of Flower-like Ag-ZnO Nanostructure and Its Application in the Photodegradation of Methyl Orange. *J. Braz. Chem. Soc.* **2013**, *24*, 1329−1338.
(72) Chen, X.; Wu, Z.; Liu, D.; Gao, Z. Preparation of ZnO Photocatalyst for the Efficient and Rapid Photocatalytic Degradation of Azo Dyes. *Nanoscale Res. Lett.* **2017**, *12*, 4−13.

https://dx.doi.org/10.1021/acsomega.0c05092
ACS Omega 2021, 6, 1426−1435